Applied Physics Letters

RESEARCH ARTICLE | MARCH 06 2024

Development of prototype system for quantum two-way clock synchronization

Bingke Shi ; Xiao Xiang ; Huibo Hong ; Yuting Liu; Pengfei Zhang; Runai Quan ; Tao Liu ; Mingtao Cao; Shougang Zhang; Ruifang Dong

Check for updates

Appl. Phys. Lett. 124, 104001 (2024)
https://doi.org/10.1063/5.0191453

View Online
Export Citation

15 April 2024 16:23:04

AIP Publishing

HIDEN ANALYTICAL
Instruments for Advanced Science
Knowledge
Experience
Expertise
Click to view our product catalogue
Contact Hiden Analytical for further details:
www.HidenAnalytical.com
info@hiden.co.uk
Gas Analysis
dynamic measurement of reaction gas streams
catalysis and thermal analysis
molecular beam studies
dissolved species probes
fermentation, environmental and ecological studies
Surface Science
UHV TPD
SIMS
end point detection in ion beam etch
elemental imaging - surface mapping
Plasma Diagnostics
plasma source characterization
etch and deposition process reaction kinetic studies
analysis of neutral and radical species
Vacuum Analysis
partial pressure measurement and control of process gases
reactive sputter process control
vacuum diagnostics
vacuum coating process monitoring

Development of prototype system for quantum two-way clock synchronization

Cite as: Appl. Phys. Lett. **124**, 104001 (2024); doi: 10.1063/5.0191453
Submitted: 14 December 2023 · Accepted: 19 February 2024 ·
Published Online: 6 March 2024

View Online Export Citation CrossMark

Bingke Shi,[1,2] Xiao Xiang,[1] Huibo Hong,[1,2] Yuting Liu,[1,2] Pengfei Zhang,[1] Runai Quan,[1] Tao Liu,[1,2] Mingtao Cao,[1,2] Shougang Zhang,[1,2] and Ruifang Dong[1,2,3,a)]

AFFILIATIONS

[1]Key Laboratory of Time Reference and Applications, National Time Service Center, Chinese Academy of Sciences, Xi'an 710600, China
[2]School of Astronomy and Space Science, University of Chinese Academy of Sciences, Beijing 100049, China
[3]Hefei National Laboratory, Hefei 230088, China

[a)]Author to whom correspondence should be addressed: dongruifang@ntsc.ac.cn

ABSTRACT

In this Letter, we report a prototype system that realizes the complete functionality for quantum two-way time transfer, comparison, and synchronization between two integrated terminals. The synchronization performance was tested over a 50-km spooled fiber link. With the common frequency reference, the time deviation was measured as 0.45 ps at an averaging time of 10^4 s, which is limited by the system's hardware and determines the minimum achievable synchronization stability. By employing an open-loop fiber-optic microwave frequency transfer in combination with the technique of dynamically identifying and steering the time offset between the terminals, a synchronization stability of 1.26 ps at 10^4 s was achieved. Further utilizing the grey prediction model to correct the time offset data, the synchronization stability was significantly improved to 0.69 ps at 10^4 s, showing its potential to enhance the synchronization performance. This report marks the development of a utility quantum two-way clock synchronization system. The ongoing exploration of advanced time-offset adjustment strategies to attain synchronization stability significantly below 1 ps is poised to yield invaluable benefits for future applications.

© 2024 Author(s). All article content, except where otherwise noted, is licensed under a Creative Commons Attribution (CC BY) license (http://creativecommons.org/licenses/by/4.0/). https://doi.org/10.1063/5.0191453

15 April 2024 16:23:04

With the rapid development of emerging atomic frequency standards, clock synchronization has increasingly demonstrated its significant role in fundamental research and engineering applications,[1–3] including precise navigation and positioning, radio astronomy, as well as cutting-edge quantum information processing and networks.[4–6] The two-way time transfer (TWTT) technique[7] has shown advantages in practical applications as it cancels out the substantial impact of link delays and their associated fluctuations, thereby eliminating the requirement for complex feedback compensation structures. In addition, the security of time transfer has been recognized as a crucial issue since any malicious spoofing may lead to malfunctions of the key facilities relying on precise timing.[8] The utilization of TWTT has been proven necessary for detecting man-in-the-middle (MITM) delay attacks.[9,10] Benefiting from the low-loss and high-reliability of optical fiber, the TWTT over fibers[11–16] has demonstrated superior precision in time and frequency synchronization compared to their satellite-based counterparts.[17–19] However, due to the inherent classical noise, the precision of both the space-based and fiber-based TWTT methods is limited to the picosecond level. To enhance its precision and security attributes, various quantum time transfer protocols have been proposed and substantiated through proof-of-principle experiments.[20–30] The quantum TWTT (Q-TWTT) protocol[23,27] utilizes energy-time entangled biphoton sources as carriers of timing signals, and the difference between the photons' sending and arriving time at the receiver can be precisely determined.[4]

In combination with high-precision nonlocal correlation identification[4,31,32] and efficient nonlocal dispersion cancelation techniques,[33] experimental demonstrations conducted over laboratory fiber links have achieved time transfer stability better than 100 fs.[27,34] Extensions to real-world scenarios have also been implemented with stability well below 1 ps over both free-space and urban fiber link, despite significant losses of more than 30 dB.[35,36] Recently, researchers have conducted detailed numerical simulations to explore the feasibility of utilizing quantum resources on satellites for time distribution, indicating the potential for establishing a high-precision global synchronization network through quantum entanglement.[37] All these achievements have

© Author(s) 2024

showcased the bright prospect of quantum clock synchronization for practical applications. However, most of the reported works were proof-of-principle demonstrations without fully considering the physical operations of realizing the complete function of quantum clock synchronization and its applicability in existing systems.

In this Letter, we present a utility prototype system, which operates the Q-TWTT in a plug-and-play fashion and realizes the complete functionality for time transfer, comparison, and synchronization. As a major improvement, the synchronized time and frequency signals are physically accessible for further practical applications. At the cost of slightly compromising the precision and efficiency of photon counting and temporal correlation measurement, all hardware components necessary for prepare-and-measure operation have been consolidated within a single terminal. With two such terminals linked by a 50-km coiled single-mode fiber (ITU-T G.652), a point-to-point quantum two-way clock synchronization system was demonstrated. By applying the open-loop fiber-optic microwave frequency transfer and dynamically steering the identified time offset, the quantum two-way clock synchronization was achieved, showing a TDEV of 1.26 ps at 10^4 s. To further improve the synchronization performance, the first-order, one variable grey model [GM(1,1)][38] was employed, which offers the capability of predicting the variation of the time offset. By applying the GM prediction-based correction to the time-offset results, the TDEV was significantly reduced, achieving 0.69 ps at 10^4 s. This progress provides a direction for optimizing the dynamic time offset adjustment strategy to achieve synchronization stability far below 1 ps. This work signifies an initial completion of implementing a real-time quantum two-way clock synchronization system, which runs in a plug-and-play mode and has good applicability in existing systems.

Figure 1 depicts the physical composition of the presented prototype system based on the Q-TWTT protocol. We have adopted a compact and lightweight design, with each of the two terminals (marked as A and B) enclosed in a 4U chassis. The all-fiber energy-time entangled biphoton sources (denoted as SPDC1 and SPDC2, respectively, for the two terminals) were self-developed based on the spontaneous parametric downconversion (SPDC) process. Paired signal and idler photons were produced from a type-II periodically poled lithium niobate (PPLN) waveguide, pumped by a single-mode fiber pigtailed laser diode at 780 nm.[39] Despite the center wavelength of SPDC1 and SPDC2 is both set to be around 1563.6 nm, the difference in PPLN length results inconsistent spectral widths of 1 and 1.7 nm in full width at half maximum (FWHM), see Fig. S2 for details in the supplementary material. The Fig. S2 gives detailed information for the previous sentence. Instead of using the high-performance but bulky superconducting nanowire single-photon detectors, the compact InGaAs/InP single-photon detectors (QCD-600B-S, QuantumCTek, SPD1&SPD2) were used for single photon detection despite their rather lower efficiency (∼25%), larger temporal jitter (∼150 ps), and higher dark count rates (∼2 kHz). The single-mode-multimode fiber combiners (SMMFCs) were adopted to ensure that the individual single-photon detector simultaneously records the photons maintained in the local terminal and those received from the remote terminal.

As shown in Fig. 1, the idler photons (i_1) from SPDC1 in terminal A are detected locally by SPD1, while the paired signal photons (s_1) are transmitted through the fiber-optic link to terminal B and detected by SPD2. The arrival times of the photons, denoted as $t_{1,A}$ and $t_{1,B}$, are then tagged by two individual time tagger units (TTU A/TTU B, Time Tagger Ultra, Swabian Instruments), which are referenced to their local time references. Similarly, the emitted idler photons (i_2) from SPDC2 at terminal B are locally detected by D2 after being combined with s_1 by SMMFC2, while the signal photons (s_2) travel through the same fiber link in the opposite direction and are then co-detected with i_1 in terminal A. The arrival times of the photons from SPDC2 are denoted as $t_{2,A}$ and $t_{2,B}$, respectively. Through the equipped optical circulators (OC1 and OC2) in each terminal, the forward and backward signal photons (s_1 and s_2) are able to share the same fiber-optic link. To nonlocally compensate for the dispersion encountered by the signal photons traveling through the 50-km fiber link, two fiber Bragg grating-based dispersion compensation modules (DCM1/DCM2, DCMCB-SN-050P1FA, Proximion, Inc.) were applied to the idler photon paths.

To simplify the time difference identification of $t_{1,B} - t_{1,A}$ and $t_{2,A} - t_{2,B}$, the photon events detected by SPD1 and SPD2 are individually divided into two portions using a power splitter (PS, ZFRSC-42-S+, Mini-Circuits). The two outputs in each terminal are then parallely connected to channels 1 and 2 of its equipped TTU. The

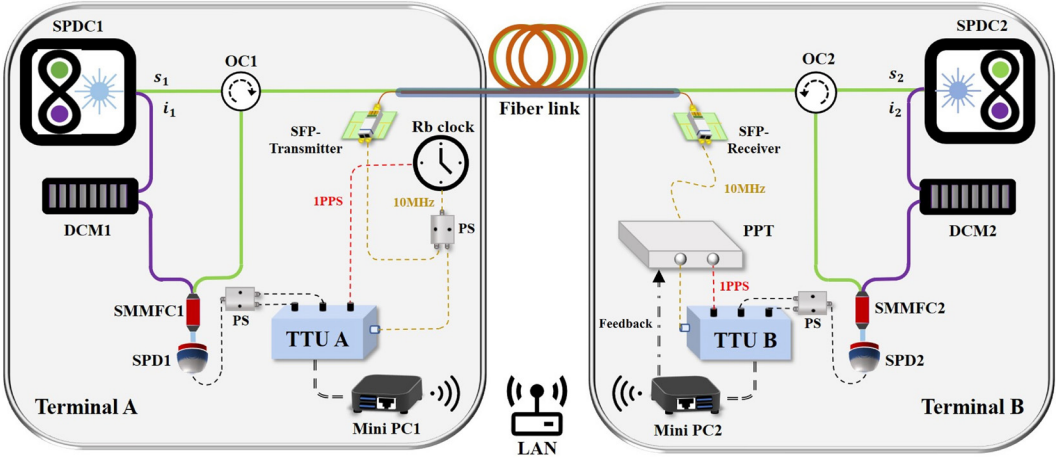

FIG. 1. Schematic diagram of the prototype system setup for quantum two-way clock synchronization.

15 April 2024 16:23:04

© Author(s) 2024

open-loop fiber-optic microwave frequency transfer scheme is applied rather than using two independent time references. The 10 MHz frequency signal from a commercial Rb clock (PRS10, Stanford Research Systems) is equipped in terminal A as the frequency reference of TTU A. At the same time, it is encoded onto a small form-factor pluggable (SFP, 0.4 mW@1450 nm, HXSC-1LF41C, Walsun Technology Ltd) module and directly transferred through a coaxial 50-km fiber to terminal B, where it is decoded out via another SFP module and used as the frequency reference of TTU B after being adjusted by the equipped programmable phase trimmer (PPT, Synchronization Technology Ltd). To establish the timestamp references for TTU A and TTU B, two 1PPS (pulse per second) time signals homologous to their respective 10 MHz frequency references are generated. They are then tagged by TTU A and TTU B, respectively, and denoted as $t_{0,A}$ and $t_{0,B}$. The mini personal computers (mini PC1 & mini PC2), which are connected through LAN, are used to store and process the recorded timestamps.

The whole operational structure comprises a hardware layer and a software layer. The hardware layer includes the above-mentioned components, facilitating input/output connections and peripheral device access. The software layer, executed in a Python environment with a graphical user interface (GUI), handles tasks, such as command transmission, data analysis, and visualization. Specifically, upon receiving the command to begin operations via the LAN and TCP/IP, both TTUs commence periodic tagging of photon arrival times [$t_{1(2),A}$ and $t_{1(2),B}$] as well as the 1PPS signals generated from their respective frequency references ($t_{0,A}$ and $t_{0,B}$). Each tagging period lasts for 10 s, during which the recorded timestamp sequences are stored as data file packages in the mini PCs. The stored data file packages in the mini PCs are transferred via the LAN to the central processor. For our experiment, mini PC2 is designated as the central processor. The central processor merges the received data file packages to identify the coincidence histograms of $G^{(2)}(t_{1,B}, t_{1,A})$ and $G^{(2)}(t_{2,A}, t_{2,B})$. The time differences $t_{1,B} - t_{1,A}$ and $t_{2,A} - t_{2,B}$ for registration are obtained through automatic Gaussian fitting. According to the Q-TWTT principle, the time offset can be determined with $t_0 = \frac{(t_{1,B}-t_{1,A})-(t_{2,A}-t_{2,B})}{2}$ and then provided to the PPT in terminal B to facilitate the synchronization between the 1PPS signals.

Due to the initially free-running mode of terminal A and terminal B, an inevitable gap between the individual start recording times would degrade the number of valid timestamps for the nonlocal temporal correlation identification. To resolve this issue, two pre-synchronized 1PPS time signals ($t_{0,A}$ and $t_{0,B}$) were tagged along with the photons, offering an opportunity for determining the time gap between the two data packets within 100 ns accuracy. In practical time distribution systems, this coarse pre-synchronization process can be easily achieved by alternative means, such as satellite timing protocol.[40] The recorded timestamps by TTUs within a tagging period are displayed in Fig. 2. Channels −1 and −2 correspond to the first and second channels of TTU A, which are used to record the photon arrival times of $t_{1,A}$ and $t_{2,A}$. The negative sign denotes that the falling edge triggers the channel. Channel 4 of TTU A is used to record the 1PPS signal. To distinguish the channels between TTUs, the first, second, and 1PPS signal channels of TTU B are labeled as −5, −6, and 8, respectively. As observed in Fig. 2, there is a time gap of approximately 500 ms between the 1PPS signals of TTU A and TTU B. Subsequently, the coarse pre-synchronization is performed by aligning all the recorded timestamps of TTU B as shown by Fig. 2(b).

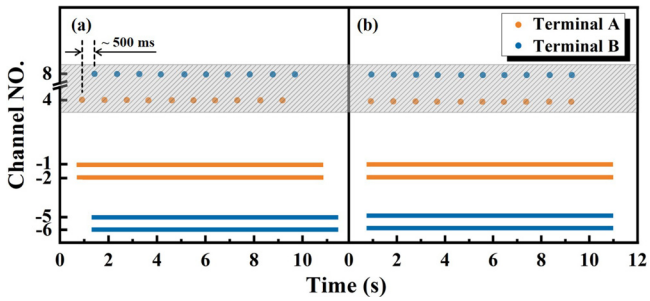

FIG. 2. The timestamps recorded by both TTUs within a 10-s tagging period before (a) and after (b) the coarse pre-synchronization process.

The system performance in time-offset measurement was first evaluated by applying the 10 MHz signal of the Rb clock as the common frequency reference to TTU A and TTU B. Following the procedure described above, the correlation distributions of $G^{(2)}(t_{1,B}, t_{1,A})$ and $G^{(2)}(t_{2,A}, t_{2,B})$ are presented in Fig. 3(a) as red dots and green squares, respectively. The correlation peak positions of $t_{1,B} - t_{1,A}$ and $t_{2,A} - t_{2,B}$, along with FWHM being 193.5 and 313.2 ps were obtained, respectively, by Gaussian fitting. The imbalance between the two coincidence distributions is mainly due to the inconsistent spectral width of the SPDC1 and SPDC2. The corresponding delays were compensated for ensuring the simultaneous occurrence of the two correlation peaks within a fixed window. The time offset of t_0 was determined by substituting the Gaussian fitted peak positions of $(t_{1,B} - t_{1,A})$ and $(t_{2,A} - t_{2,B})$ into the following equation: $t_0 = \frac{(t_{1,B}-t_{1,A})-(t_{2,A}-t_{2,B})}{2}$. Figure 3(b) shows the variation of t_0 with the measurement time lasting for 40 000 s, which has a standard deviation (STD) of 3.3 ps and a slight linear fitted slope of -2.1×10^{-5} ps/s.

Further replacing the common frequency reference with utilizing the open-loop fiber-optic microwave frequency transfer, the identified correlation distributions are shown in Fig. 3(c). In comparison with Fig. 3(a), these distributions exhibit a slight decrease in coincidence counts, which could be related to the different photon counts in the two

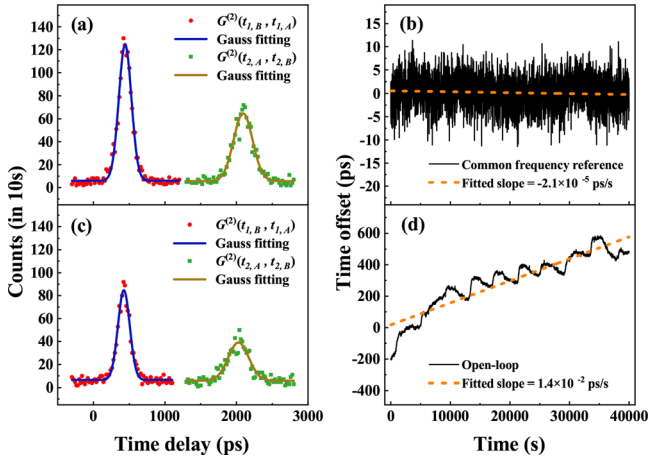

FIG. 3. The identified correlation distributions and long-term variation of the measured time offset when a common frequency reference (a) and (b) and an open-loop fiber-optic microwave frequency transfer (c) and (d) are applied, respectively.

15 April 2024 16:23:04

© Author(s) 2024

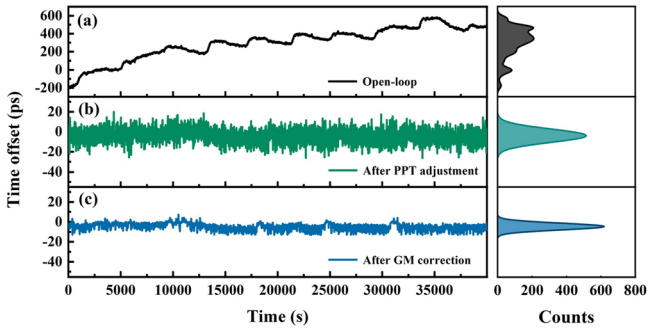

FIG. 4. Variations of the measured time offsets in cases of open-loop (a), after real-time adjustment by the PPT (b), and after the prediction-based correction using GM (1,1) (c).

separate implementations. However, the coincidence widths remain unchanged, indicating that the open-loop fiber-optic microwave frequency transfer is able to provide a short-term common frequency reference for measuring time offsets. The corresponding long-term measurement of the time offset t_0 is plotted in Fig. 3(d). A significant drift up to 0.8 ns and a slope of 1.4×10^{-2} ps/s within 40 000 s is observed, which could be attributed to the uncontrolled delay variation in the open-loop fiber-optic microwave frequency transfer.

To remove the time-varying drift, phase adjusting via the equipped PPT in terminal B was implemented. A proportional coefficient (0.3) was introduced for phase adjustment based on the last measured time offset, as to prevent excessive feedback resulting in oscillations in the adjusted time offset. The resultant time offset after the real-time phase adjustment as a function of the measurement time is shown in Fig. 4(b). For comparison, the variation of the time offsets with the measurement time is also shown in Fig. 4(a), whose histogram is plotted in the right-hand and gives a STD of 173.87 ps. In comparison with the open-loop case, the apparent drift was efficiently eliminated and the STD was decreased to 6.67 ps. To further reduce the fluctuations, a more advanced algorithm than simply applying the proportional phase adjustment is desired.

The grey model has been widely used in atomic clock modeling and satellite clock prediction[41,42] for enhancing time and frequency transfer performances. As a preliminary attempt, we employed the first-order, one-variable grey model (GM(1, 1))[38] to perform prediction-based correction to the PPT-adjusted time-offset results. The length of the sampling window, which represents the number of involved data points for predicting the trend of the next data, was chosen to be 20 in the prediction process. The correction is implemented by comparing the measured ($t_{0,meas}$) and predicted ($t_{0,pred}$) time offsets, once the weighted deviation ($|t_{0,meas} - t_{0,pred}|/t_{0,meas}$) surpasses a threshold (0.5), $t_{0,meas}$ will be replaced by $t_{0,pred}$. Upon correction using the GM prediction model, the time-offset data are presented in Fig. 4(c) with the blue solid line and reveals a STD of 3.61 ps, indicating that the application of the GM prediction algorithm can substantially reduce the fluctuations observed in the PPT-adjusted time offset (see the supplementary material for further discussions).

To evaluate the synchronization stability performance under different scenarios, the time deviation (TDEV) results as functions of the averaging time are shown in Fig. 5. Under the common frequency reference, the TDEV curve (red squares) follows a descending slope of

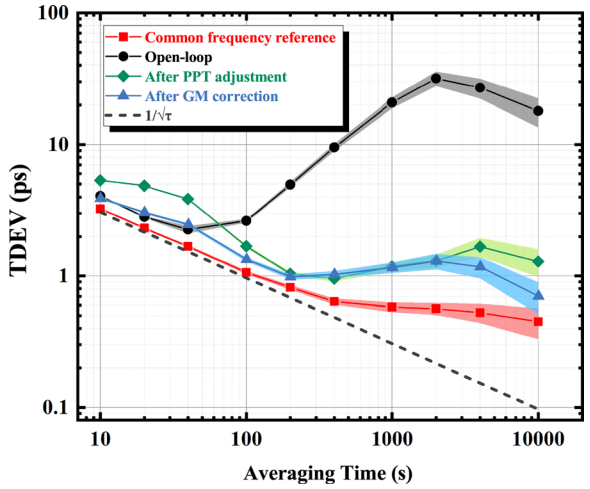

FIG. 5. Measured TDEVs for the quantum two-way clock synchronization over a 50 km-long fiber-optic link under four different scenarios.

$1/\sqrt{\tau}$ until the averaging time τ reaches 400 s. Afterward, the TDEV slope gradually flattens out, which should be due to the presence of asymmetry, such as different spectral properties of the SPDC sources. At the averaging time of 10^4 s, the TDEV reaches 0.45 ps, setting the lower limit for system synchronization stability. After replacing the common frequency reference with the open-loop fiber-optic microwave frequency transfer, the TDEV curve (black circles) presents similar short-term stability until the averaging time τ reaches 40 s, then it starts to rise as the impact of ambient fluctuations stands out in the fiber link. The inflection point of the curve occurs at 2000 s, which is attributed to periodic temperature changes in the air conditioning laboratory, resulting in a maximum TDEV of 31.83 ps. After applying the real-time PPT adjustment to the time offsets, the TDEV result is given by green diamonds. Compared with the open-loop case (black circles), a modest degradation of the short-term stability happens within the averaging time from 10 to 50 s. Afterward, a remarkable reduction of TDEV is shown from 400 to 10^4 s, resulting in a TDEV of 1.26 ps at 10^4 s. By adopting the GM(1,1) prediction to the PPT-adjusted time offsets, the potential improvement to the TDEV was also evaluated and shown by the blue triangles. We see that the TDEV in the short-term averaging regime was effectively improved, which presents a close resemblance to the descending trend of the common frequency reference case until the averaging time reaches 200 s. In the long-term averaging regime from 2000 to 10^4 s, the TDEV improvement was also achieved, resulting in a minimum of 0.69 ps at 10^4 s (see the supplementary material for details). This further affirms that the GM prediction algorithm enables the mitigation of fluctuation, benefitting from its capability of predicting the time and frequency transfer performance.

In summary, we have designed and demonstrated a plug-and-play prototype system for quantum two-way clock synchronization. By employing an open-loop fiber-optic microwave frequency transfer in combination with dynamically identifying and steering the time offset between independent terminals, a synchronization stability of 1.26 ps at 10^4 s was achieved over a 50-km spooled fiber. Further applying the GM(1,1) model, a significantly improved time stability to 0.69 ps was demonstrated, underscoring its potential efficacy of

15 April 2024 16:23:04

© Author(s) 2024

enhancing the synchronization stability. The system performance is expected to be further improved by accelerating data processing through hardware such as field programmable gate array (FPGA) and combining modified prediction models to enhance the capability of the dynamic time offset adjustment. It is worth noting that the synchronization stability of the prototype system is constrained to 0.45 ps at 10^4 s due to the inconsistent spectral width of biphoton sources and the larger SPD jitter. Through optimization of the biphoton sources and utilizing superconducting nanowire single-photon detectors for photon detection, the minimum achievable synchronization stability can be significantly improved to tens of femtoseconds,[27,34] promising a bright prospect of more superior synchronization stability.

See the supplementary material for details of physical configuration, operation structure, time offsets variations, and synchronization stability analysis.

This work was supported by the National Natural Science Foundation of China (Grant Nos. 12033007, 12103058, 61801458, 12203058, 12074309, and 61875205), the Youth Innovation Promotion Association, CAS (Grant Nos. 2022413, 2021408, and 2023425), and the China Postdoctoral Science Foundation (Grant No. 2022M723174). We wish to acknowledge Dr. Zuzeng Lin (Tianjin University, China) and Dr. Tim Wolz (Swabian Instruments GmbH, Germany) for their fruitful discussions on raw timestamp processing.

AUTHOR DECLARATIONS

Conflict of Interest

The authors have no conflicts to disclose.

Author Contributions

Bingke Shi and Xiao Xiang contributed equally to this work.

Bingke Shi: Data curation (equal); Formal analysis (equal); Investigation (equal); Methodology (equal); Writing – original draft (equal); Writing – review & editing (equal). **Xiao Xiang:** Conceptualization (equal); Data curation (equal); Investigation (equal); Methodology (equal); Writing – original draft (equal); Writing – review & editing (equal). **Huibo Hong:** Software (equal). **Yuting Liu:** Data curation (equal); Writing – review & editing (equal). **Pengfei Zhang:** Methodology (equal); Writing – review & editing (equal). **Runai Quan:** Conceptualization (equal); Investigation (equal); Writing – review & editing (equal). **Tao Liu:** Methodology (equal); Writing – review & editing (equal). **Mingtao Cao:** Conceptualization (equal); Investigation (equal); Writing – review & editing (equal). **Shougang Zhang:** Investigation (equal); Writing – review & editing (equal). **Ruifang Dong:** Conceptualization (lead); Funding acquisition (lead); Investigation (equal); Methodology (equal); Supervision (lead); Writing – original draft (equal); Writing – review & editing (equal).

DATA AVAILABILITY

The data that support the findings of this study are available from the corresponding author upon reasonable request.

REFERENCES

[1]R. N. Gore, E. Lisova, J. Åkerberg, and M. Björkman, "CoSiWiNeT: A clock synchronization algorithm for wide area IIoT network," Appl. Sci. **11**, 11985 (2021).
[2]J. N. Pelton and J. N. Pelton, *The Growth and Expansion of Precise Navigation and Timing* (Springer, 2019), pp. 47–58.
[3]M. Xin, K. Şafak, and F. X. Kärtner, "Ultra-precise timing and synchronization for large-scale scientific instruments," Optica **5**, 1564–1578 (2018).
[4]C. Spiess and F. Steinlechner, "Clock synchronization with pulsed single photon sources," Quantum Sci. Technol. **9**, 015019 (2024).
[5]J. Liu, Z. Lin, D. Liu, X. Feng, F. Liu, K. Cui, Y. Huang, and W. Zhang, "High-dimensional quantum key distribution using energy-time entanglement over 242 km partially deployed fiber," Quantum Sci. Technol. **9**, 015003 (2024).
[6]Z.-Y. Xu, J.-L. Wang, J. Teng, G.-J. Fan-Yuan, and Y.-Z. Gui, "Time-synchronization error in twin-field quantum key distribution," Phys. Rev. A **108**, 032604 (2023).
[7]J. Levine, "A review of time and frequency transfer methods," Metrologia **45**, S162 (2008).
[8]A. Jafarnia-Jahromi, A. Broumandan, J. Nielsen, and G. Lachapelle, "GPS vulnerability to spoofing threats and a review of antispoofing techniques," Int. J. Navig. Obs. **2012**, 127072.
[9]A. Lamas-Linares and J. Troupe, "Secure quantum clock synchronization," Proc. SPIE **10547**, 59–66 (2018).
[10]H. Dai, Q. Shen, C.-Z. Wang, S.-L. Li, W.-Y. Liu, W.-Q. Cai, S.-K. Liao, J.-G. Ren, J. Yin, Y.-A. Chen, Q. Zhang, F. Xu, C.-Z. Peng, and J.-W. Pan, "Towards satellite-based quantum-secure time transfer," Nat. Phys. **16**, 848–852 (2020).
[11]P. Krehlik, Å. Sliwczynski, Å. Buczek, and M. Lipinski, "Fiber-optic joint time and frequency transfer with active stabilization of the propagation delay," IEEE Trans. Instrum. Meas. **61**, 2844–2851 (2012).
[12]O. Lopez, C. Chardonnet, A. Amy-Klein, A. Kanj, P.-E. Pottie, D. Rovera, J. Achkar, and G. Santarelli, "Simultaneous remote transfer of accurate timing and optical frequency over a public fiber network," in *Joint European Frequency and Time Forum & International Frequency Control Symposium (EFTF/IFC)* (IEEE, 2013), pp. 474–476.
[13]R. Dong, X. Guo, B. Hou, B. Liu, F. Yang, W. Kong, J. Ju, T. Liu, and S. G. Zhang, "Time transfer in a 1839 km telecommunication fiber link demonstrating a picosecond-scale stability," Optica Open (published online, 2023).
[14]Q. Zhou, X. Zhang, Q. Zang, X. Deng, M. Wu, J. Liu, D. Wang, R. Dong, T. Liu, and S. Zhang, "Coherent optical frequency transfer via aerial fiber link with 10^{-19} of instability," in Joint Conference of the European Frequency and Time Forum and IEEE International Frequency Control Symposium (EFTF/IFCS), 2023.
[15]Q. Zang, X. Deng, X. Zhang, D. Wang, Q. Zhou, J. Dong, G. Xu, J. Gao, J. Liu, T. Liu, R. Dong, and S. Zhang, "Cascaded transfer of optical frequency with a relay station over a 224 km deployed fiber link," Infrared Phys. Technol. **128**, 104511 (2023).
[16]B. Liu, X. Guo, W. Kong, T. Liu, R. Dong, and S. Zhang, "Stabilized time transfer via a 1000-km optical fiber link using high-precision delay compensation system," Photonics **9**, 522 (2022).
[17]D. Piester, A. Bauch, L. Breakiron, D. Matsakis, B. Blanzano, and O. Koudelka, "Time transfer with nanosecond accuracy for the realization of international atomic time," Metrologia **45**, 185 (2008).
[18]Z. Jiang, V. Zhang, T. E. Parker, G. Petit, Y.-J. Huang, D. Piester, and J. Achkar, "Improving two-way satellite time and frequency transfer with redundant links for UTC generation," Metrologia **56**, 025005 (2019).
[19]D. Valat and J. Delporte, "Absolute calibration of timing receiver chains at the nanosecond uncertainty level for GNSS time scales monitoring," Metrologia **57**, 025019 (2020).
[20]V. Giovannetti, S. Lloyd, and L. Maccone, "Quantum-enhanced positioning and clock synchronization," Nature **412**, 417–419 (2001).
[21]T. B. Bahder and W. M. Golding, "Clock synchronization based on second-order quantum coherence of entangled photons," AIP Conf. Proc. **734**, 395–398 (2004).
[22]R. Quan, Y. Zhai, M. Wang, F. Hou, S. Wang, X. Xiang, T. Liu, S. Zhang, and R. Dong, "Demonstration of quantum synchronization based on second-order quantum coherence of entangled photons," Sci. Rep. **6**, 30453 (2016).
[23]F. Hou, R. Dong, T. Liu, and S. Zhang, "Quantum-enhanced two-way time transfer," in *Quantum Information and Measurement (QIM) 2017* (Optica Publishing Group, 2017), p. QF3A.4.
[24]R. Quan, R. Dong, Y. Zhai, F. Hou, X. Xiang, H. Zhou, C. Lv, Z. Wang, L. You, T. Liu, and S. Zhang, "Simulation and realization of a second-order quantum-interference-based quantum clock synchronization at the femtosecond level," Opt. Lett. **44**, 614–617 (2019).

15 April 2024 16:23:04

© Author(s) 2024

[25]M. Xie, H. Zhang, Z. Lin, and G.-L. Long, "Implementation of a twin-beam state-based clock synchronization system with dispersion-free hom feedback," Opt. Express **29**, 28607–28618 (2021).
[26]Y. Liu, R. Quan, X. Xiang, H. Hong, M. Cao, T. Liu, R. Dong, and S. Zhang, "Quantum clock synchronization over 20-km multiple segmented fibers with frequency-correlated photon pairs and HOM interference," Appl. Phys. Lett. **119**, 144003 (2021).
[27]F. Hou, R. Quan, R. Dong, X. Xiang, B. Li, T. Liu, X. Yang, H. Li, L. You, Z. Wang, and S. Zhang, "Fiber-optic two-way quantum time transfer with frequency-entangled pulses," Phys. Rev. A **100**, 023849 (2019).
[28]J. Lee, L. Shen, A. Cerè, J. Troupe, A. Lamas-Linares, and C. Kurtsiefer, "Symmetrical clock synchronization with time-correlated photon pairs," Appl. Phys. Lett. **114**, 101102 (2019).
[29]J. Lee, L. Shen, A. Cerè, J. Troupe, A. Lamas-Linares, and C. Kurtsiefer, "Asymmetric delay attack on an entanglement-based bidirectional clock synchronization protocol," Appl. Phys. Lett. **115**, 141101 (2019).
[30]R. Quan, H. Hong, W. Xue, H. Quan, W. Zhao, X. Xiang, Y. Liu, M. Cao, T. Liu, S.-G. Zhang, and R. Dong, "Implementation of field two-way quantum synchronization of distant clocks across a 7 km deployed fiber link," Opt. Express **30**, 10269 (2022).
[31]R. Quan, R. Dong, X. Xiang, B. Li, T. Liu, and S. Zhang, "High-precision nonlocal temporal correlation identification of entangled photon pairs for quantum clock synchronization," Rev. Sci. Instrum. **91**, 123109 (2020).
[32]C. Spiess, S. Töpfer, S. Sharma, A. Kržič, M. Cabrejo-Ponce, U. Chandrashekara, N. L. Döll, D. Rieländer, and F. Steinlechner, "Clock synchronization with correlated photons," Phys. Rev. Appl. **19**, 054082 (2023).
[33]X. Xiang, R. Quan, Y. Liu, B. Shi, H. Hong, Y. Jin, T. Liu, R. Dong, and S. Zhang, "Widely flexible and finely adjustable nonlocal dispersion cancellation with wavelength tuning," Opt. Express **30**, 44487–44495 (2022).
[34]H. Hong, R. Quan, X. Xiang, W. Xue, H. Quan, W. Zhao, Y. Liu, M. Cao, T. Liu, S. Zhang, and R. Dong, "Demonstration of 50 km fiber-optic two-way quantum clock synchronization," J. Lightwave Technol. **40**, 3723–3728 (2022).
[35]H. Hong, R. Quan, X. Xiang, Y. Liu, T. Liu, M. Cao, R. Dong, and S. Zhang, "Quantum two-way time transfer over a 103 km urban fiber," J. Lightwave Technol. (published online, 2024).
[36]X. Xiang, B. Shi, R. Quan, Y. Liu, Z. Xia, H. Hong, T. Liu, J. Wu, J. Qiang, J. Jia, S. Zhang, and R. Dong, "Quantum two-way time transfer over a hybrid free-space and fiber link," Quantum Sci. Technol. **8**, 045017 (2023).
[37]S. Haldar, I. Agullo, A. J. Brady, A. Lamas-Linares, W. C. Proctor, and J. E. Troupe, "Towards global time distribution via satellite-based sources of entangled photons," Phys. Rev. A **107**, 022615 (2023).
[38]S. Liu, Y. Yang, and J. Forrest, "Series of GM models," in *Grey Data Analysis: Methods, Models and Applications* (Springer Singapore, Singapore, 2017), pp. 141–181.
[39]Y. Liu, J. Xing, Z. Xia, R. Quan, H. Hong, T. Liu, S. Zhang, X. Xiang, and R. Dong, "All-fiber telecom band energy-time entangled biphoton source," Chin. Opt. Lett. **21**, 032701 (2023).
[40]P. Johnson, A. Novick, and M. Lombardi, "Measuring the timing accuracy of satellite time and location (STL) receivers," in *Proceedings of the Precise Time and Time Interval (PTTI) Meeting* (2023), pp. 207–215.
[41]P. Zhang, R. Tu, Y. Gao, and R. Zhang, "Atomic clock modelling augmenting time and frequency transfer using carrier phase observation," in IET Radar, Sonar and Navigation, 2020, Vol. 14.
[42]X. Tan, J. Xu, F. Li, M. Wu, D. Chen, and Y. Liang, "A new GM (1,1) model suitable for short term prediction of satellite clock bias," in IET Radar, Sonar and Navigation, 2022, Vol. 16.

15 April 2024 16:23:04

© Author(s) 2024